MITSUBISHI ELECTRIC RESEARCH LABORATORIES
http://www.merl.com

A generic model for MIMO wireless propagation channels in macro- and microcells

Molisch, A.

TR2003-42 May 2003

Abstract

This paper derives a generic model for the MIMO wireless channel. The model has the ability to explain important effects, including (i) interdependency of directions-of-arrival and directions-of-departure, (ii) large delay and angle dispersion by propagation via far clusters, (iii) rank reduction of the transfer function matrix. We propose a geometry-based model that includes the propagation effects that are critical for MIMO performance: (i) single scattering around the BS and MS, (ii) scattering by far clusters, (iii) double-scattering, (iv) waveguiding, and (v) diffraction by roof edges. The required parameters for the complete definition of the model are enumerated, and typical parameter values in macro- and microcellular environments are discussed.

MERL – A MITSUBISHI ELECTRIC RESEARCH LABORATORY
http://www.merl.com

A generic model for MIMO wireless propagation channels in macro- and microcells

Andreas F. Molisch

TR-2003-42 May 2003

Abstract

This paper derives a generic model for the MIMO wireless channel. The model has the ability to explain important effects, including (i) interdependency of directions-of-arrival and directions-of-departure, (ii) large delay and angle dispersion by propagation via far clusters, (iii) rank reduction of the transfer function matrix. We propose a geometry-based model that includes the propagation effects that are critical for MIMO performance: (i) single scattering around the BS and MS, (ii) scattering by far clusters, (iii) double-scattering, (iv) waveguiding, and (v) diffraction by roof edges. The required parameters for the complete definition of the model are enumerated, and typical parameter values in macro- and microcellular environments are discussed.

Publication History:

1. First printing, TR-2003-42, May 2003

A generic model for MIMO wireless propagation channels in macro- and microcells

Andreas F. Molisch *Senior Member, IEEE*

Part of this work was presented at ICC 2002 and VTC spring 2002.

A. F. Molisch was with the ”Wireless Systems Research Department”, AT&T Labs - Research, Middletown, NJ, USA. He is now with Mitsubishi Electric Research Laboratories - Murray Hill Labs, Murray Hill, NJ and the Department of Electroscience, Lund University, Lund, Sweden. E-mail: Andreas.Molisch@ieee.org.

Abstract

This paper derives a generic model for the MIMO wireless channel. The model has the ability to explain important effects, including (i) interdependency of directions-of-arrival and directions-of-departure, (ii) large delay and angle dispersion by propagation via far clusters, (iii) rank reduction of the transfer function matrix. We propose a geometry-based model that includes the propagation effects that are critical for MIMO performance: (i) single scattering around the BS and MS, (ii) scattering by far clusters, (iii) double-scattering, (iv) waveguiding, and (v) diffraction by roof edges. The required parameters for the complete definition of the model are enumerated, and typical parameter values in macro- and microcellular environments are discussed.

Index Terms

MIMO, channel model, keyholes, dispersion

I. INTRODUCTION

In the last years, MIMO (multiple-input - multiple-output) systems have emerged as one of the most promising approaches for high-datarate wireless systems [1], [2]. In principle, the infomation-theoretic capacity of these systems can increase linearly with the number of antennas. In order to achieve or at least approach those capacities, sophisticated signal processing algorithms (like BLAST [3]) and coding strategies [4] have been developed, and research on those topics continues. In order to assess the benefits and possible problems of all those algorithms, realistic models of the wireless propagation channel are required. Since MIMO systems make use of the spatial (directional) information, those models have to include the DOAs (Directions of Arrival) and DODs (Directions of Departure) of the multipath components. For this reason, conventional channel models [5] cannot be used, and new models have to be developed.

These new channel models require two steps: (i) setting up a generic channel model and identifying the parameters that have to be determined for its description and (ii) actually performing the measurement campaigns, and extracting numerical values for the parameters. At the moment, there are not many MIMO measurement campaign results publicly available, but this is going to change in the next years. In order to allow maximum benefits from those campaigns, the first step, namely the setting up of a generic channel model, is urgently required. This paper provides such a model, as well as a preliminary parameterization.

For the standard narrowband channels, the generic model consists of an attenuator with a prescribed Doppler spectrum (time variance of the attenuation) [6]. In the wideband case, a tapped-delay line (with possibly different) Doppler spectra for each tap has been proposed in the 1960s, and is used in the COST 207 (GSM) [7] and ITU-R [8] channel models. The much more involved generic framework of the "single-directional channel", either based on a geometric or a purely stochastic approach, was established in the mid- and late 1990s [9]. All those generic models are now well-established, even though we note that the actual *values* of the parameters are still subject to discussion for different environments.

There are also some MIMO channel models available in the literature, but they are essentially constructions suited to specifically reproduce a certain effect. The most simple, and still most widely used, model is the independent Rayleigh fading at all antenna elements, introduced in [1] and also used in [2]. Subsequently, [10] [11] have analyzed the effect of correlation. It used a geometrically- based stochastic approach, placing scatterers[1] at random around the MS - a model that dates back to the early 70s [12], [13]. The implications of a more general, cluster-based model introduced in [14] were analyzed by [15]. A similar model is also currently under consideration within 3GPP and 3GPP2[16], the standardization bodies for third-generation cellular systems. In contrast to these geometry-based models, the papers [17] and [18] directly modeled the correlation matrix of the signals at the different antenna elements and introduce the simplification that scattering at transmitter and receiver is independent.Ref.[19] also includes the Doppler effect. All those models were based on the assumption that only single-scattering processes occurred, or that at least all those processes could be represented adequately by "equivalent" single-scattering processes (complex Gaussian fading of the entries of the transfer function matrix). However, the analysis of a group from Stanford [20] and one from Bell-Labs [21] showed the occurrence of so-called "keyhole-" or "pinhole-" channels whose behavior could not be explained adequately in terms of single scattering. To wit, low-rank channel transfer matrices are possible even when the entries into those matrices are uncorrelated. [20] also gave a channel model that could explain the behavior by decomposing the channel correlation matrix into three terms. The papers [22] and [23] investigated the influence of polarization. The model of [24] is mainly suitable for experimental

[1] Strictly speaking, one needs to distinguish between specular reflection and diffuse scattering, as those are different propagation processes. In this paper, however, we will use the expression "scattering" and "scatterers" to encompass both those effects.

analysis and site-specific modeling.The review paper [18] gives a more detailed look at those different channel models. Finally, we mention the virtual channel model of Sayeed [25],which is a method for describing the effect of the channel on specific systems. It describes the channel transfer matrix in a beamspace whose resolution depends on the antenna configuration. It is thus more a system analysis tool than a propagation model, and can be used in conjunction with our model.

None of the above models is general enough for explaining the wide variety of channel-induced effects in MIMO systems. This paper develops a new model for outdoor propagation (macro- and microcells) that remedies this situation. It is based on a geometric approach, combined with physical arguments about the relevant propagation effects. In section II, we discuss various methods for describing the wireless channel. Section III outlines the model structure and describes the underlying propagation effects in detail. Section IV discusses some implementation aspects and summarizes typical parameter values in macro- and microcellular environments. A summary concludes this paper.

II. CHANNEL DESCRIPTION METHODS

MIMO channels can be modeled either as double-directional channels [24] or as vector (matrix) channels [2]. The former method is more related to the physical propagation effects, while the latter is more centered on the effect of the channel on the system. Still, they must be equivalent, as they describe the same physical channel. Another distinction is whether to treat the channel deterministically or stochastically. In the following, we outline the relations between those description methods.

The *deterministic double-directional channel* is characterized by its double-directional impulse response. It consists of N propagation paths between the transmitter and the receiver sites. Each path is delayed in accordance to its excess-delay τ_ℓ, weighted with the proper complex amplitude $\underline{a}_\ell e^{j\phi_\ell}$. Note that the amplitude is a two-by-two matrix, since it describes the vertical and horizontal polarizations and the cross-polarization; neglecting a third possible polarization direction is admissible in macro- and microcells. Finally, the paths are characterized by their direction-of-departure (DOD) $\Omega_{T,\ell}$ and direction-of-arrival (DOA) $\Omega_{R,\ell}$.[2] The channel impulse response matrix $\underline{h}$,

[2]We stress that the (double-directional) channel is reciprocal. While the directions of multipath components at the base station and at the mobile station are different, the directions at one link end for the transmit case and the receive case must be identical. When we talk in the

describing horizontal and vertical polarization is then

$$\underline{h}(t,\tau,\Omega_T,\Omega_R)=\sum_{\ell=1}^{N}\underline{h}_\ell(t,\tau,\Omega_T,\Omega_R)=\sum_{\ell=1}^{N}\underline{a}_\ell e^{j\phi_\ell}\delta(\tau-\tau_\ell)\delta(\Omega-\Omega_{T,\ell})\delta(\Psi-\Omega_{R,\ell}) \quad (1)$$

The number of paths N can become very large if all possible paths are taken into account; in the limit, the sum has to be replaced by an integral. For practical purposes, paths that are significantly weaker than the considered noise level can be neglected. Furthermore, paths with similar DOAs, DODs, and delays can also be merged into "effective" paths. Note that the parameters of those paths must be similar enough so that over the distances of interest for the simulation, no fading is created by the superposition of the subpaths.

In general, all multipath parameters in (1), $\tau_\ell, \Omega_{R,\ell}$, $\Omega_{T,\ell}, \underline{a}_\ell$, and $e^{j\phi_\ell}$ will depend on the absolute time t; also the set of multipath components (MPCs) contributing to the propagation will vary, $N \rightarrow N(t)$. The variations with time can occur both because of movements of scatterers, and movement of the mobile station MS (the BS is assumed fixed). Without restriction of generality, the reference coordinate (center) of the base station antenna array is chosen to coincide with the origin of the coordinate system. We furthermore assume that the antenna arrays both at the BS and MS are small enough so that the MPC parameters do not change over the size of this array.

The *deterministic* wideband *matrix* channel response describes the channel from a transmit to a receive antenna array. It is characterized by a matrix $\underline{H}$ whose elements H_{ij} are the (nondirectoinal) impulse responses from the $j-$th transmit to the i-th receive antenna element. They can be computed for any antenna constellation as

$$H_{i,j}=h(\tau,\overrightarrow{x}_{R,i},\overrightarrow{x}_{T,j})=\sum_{\ell=1}^{N}\overrightarrow{g}_R(\Omega_R)\cdot\underline{h}(\tau_\ell,\Omega_{R,\ell},\Omega_{T,\ell})\cdot\overrightarrow{g}_T(\Omega_T)\cdot\ e^{j\left\langle\vec{k}(\varphi_{R,\ell})\vec{x}_{R,i}\right\rangle}e^{j\left\langle\vec{k}(\varphi_{T,\ell})\vec{x}_{T,j}\right\rangle}, \quad (2)$$

where where $\vec{x}_R$ and $\vec{x}_T$ are the vectors of the chosen element-position measured from an arbitrary but fixed reference points $\vec{x}_{R,0}$ and $\vec{x}_{T,0}$ (e.g., the centers of the arrays) and $\vec{k}$ is the wavevector so that

$$\left\langle\vec{k}(\Omega)\cdot\vec{x}\right\rangle=\frac{2\pi}{\lambda}(x\cos\vartheta\cos\varphi+y\cos\vartheta\sin\varphi+z\sin\vartheta). \quad (3)$$

where ϑ and φ denote elevation and azimuth, respectively.The functions $\overrightarrow{g}_R(\Omega_R)$ and $\overrightarrow{g}_T(\Omega_T)$ are the antenna patterns at transmitter and receiver, respectively, where the two entries of the vector $\overrightarrow{g}$ describe the antenna pattern for horizontal and vertical polarization.

following about DOAs and DODs, we refer to the directions at two different link ends.

The above *double-directional* description seems rather straightforward. However, a straightforward *stochastic* description of the involved parameters involves a four-dimensional probability density function that could only be described or saved as a huge file. Note that in general, the statistics of MPC delays, DOAs, DODs, amplitudes and phases are not separable, and thus have to be described by their *joint* probability density function. As we will see later on, even the common assumptions of Rayleigh-distributed amplitudes and uniformly distributed phases of the multipath components are too restrictive, as they cannot reproduce the important ”keyhole” effect.

The *stochastic* description of the *matrix channel* also seems simple at first glance. It requires the average powers of the entries of the transfer matrix (from each transmit to each receive antenna), as well as the correlation between the matrix entries. Especially for small antenna array sizes, a description of the H-matrix seems desirable. However, we have to keep the following point in mind:

1) The fading at the different antenna elements can be Rayleigh, Rician, or ”double-Rayleigh” (as shown below). Thus, we have to define those statistics and its associated parameters.
2) The number of involved correlation coefficients increases quadratically with the number of antenna elements. Their number might be reduced in periodic structures, as can be usually found at base stations (BSs) (Toeplitz structure of the correlation matrix for antenna arrays), but not necessarily for diversity arrangements as found at the mobile station (MS).
3) The whole description is dependent on the used antenna arrangement. Generalizations to larger (or just different) structures are not easily possible.
4) In delay-dispersive environments, we have to define different correlation factors for each delay, because different propagation mechanisms (which induce different correlation factors) have different delays.

In order to avoid these problems, it is necessary to come up with a new model that allows some simplifications, but is still general enough to include clustering, waveguiding, etc. The model developed in the following sections emulates the physical propagation processes that are important for MIMO systems, employing a combination of geometric and stochastic channel descriptions. .

III. BASIC STRUCTURE OF THE MODEL

The basic idea of our approach is to place scatterers at random, and then to emulate the progation processes from transmitter to receiver. The model has thus some basic similarity with a ray-tracing approach. The difference is that for true ray tracing, the location of the scatterers is taken from a geographical/morphological database, while for our approach, they are taken from a statistical distribution. In principle, our model uses a finite number of reflections at discrete point scatterers, and can be configured in such a way that an arbitrary finite, number of reflection/scattering/diffraction processes can occur between transmitter and receiver[3] - again in analogy to true ray tracing.

The idea of combining stochastic placement of scatterers with simplified ray tracing has been used successfully in the past. Rappaport and co-workers [26], [27] suggested the "single-bounce geometrical channel model" (SBGC), where scatterers are either placed uniformly in the considered cell, or located in a disk around the MS. Similar approaches were suggested independently by Blanz [28] and Fuhl et al. [14], who called it "Geometry-based Stochastic Channel Model" (GSCM), the name we will use henceforth. Reference [14] also suggested that in addition to a cluster of scatterers around the MS, so-called "far clusters" exist, which correspond to high-rise buildings or mountains.

The purpose of these models was the simulation of angular spectra for the simulations of multiple-antenna elements at the BS. For these systems, a correct emulation of the ADPS (angular delay power spectrum) can be obtained from a GSCM. Naturally, this is the case if single-scattering is the corresponding *physical* propagation process. However, it is also true if *multiple* scattering occurs physically. This equivalence of multiple and single scattering is due to the fact that there exists a unique transformation between the (x, y, z) coordinates of the location of scatterers (in a single-bounce model) and the delay, azimuth, and elevation of the multipath components "seen" at the BS. This equivalence was proven for the two-dimensional case ($z = 0$, no elevation) in [27], [29], and can be easily generalized to the three-dimensional case. Since we obtain a correct emulation of the ADPS, also the correlation of the signals at the different antenna elements of the BS is reproduced correctly. Note, however, that the *amplitude statistics* might not be correctly reproduced, as GSCM (with a large number of scatterers) always

[3]Diffraction and diffuse scattering can be approximated by point scatterers when "illumination functions" are used, see below.

results in Rayleigh amplitude statistics, whereas we will see below that other statistics might occur when multiple scattering is taken into account. [4]

For MIMO systems, the use of single scattering processes in the channel model is only suitable if single-scattering occurs physically. Once the location of the scatterer is fixed (in order to reproduce angle at the BS and the delay), it implicitly describes the angle of the multipath component at the MS as well. If, however, multiple-scattering processes are involved, the true angle at the MS might be different.

As mentioned above, the GSCM assumes that all propagation processes can be approximated by a finite number of reflections at discrete point scatterers. This is not a serious restriction of generality, since any propagation process can be represented in that way if the number of scatterers is chosen sufficiently large. However, in order to keep the model efficient, the number of used scatterers, and the number of considered reflection processes, should be small. For this reason, waveguiding and diffraction are described in our model by a different, phenomenological, approach.

In the following, we list the important propagation processes and their parameterization.

A. Line of sight component

The line-of-sight propagation (Fig. 1a) can be included in a straightforward way in any geometrical approach. The set of parameters $\tau, \Omega_{R,}, \Omega_T, \underline{a}e^{j\phi}$ is given as $\tau = d/c_0, \Omega_T = 0, \Omega_{R,} = \pi$ where we assume that the LOS is used as the reference line from which all DOAs and DODs are measured, and $d = |\overrightarrow{x}_{R,0} - \overrightarrow{x}_{T,0}|$ is the distance between the reference antenna points $\vec{x}_{R,0}$ and $\vec{x}_{T,0}$.. The attenuation of the LOS component is given as

$$\underline{a} = \begin{pmatrix} 1 & 0 \\ 0 & 1 \end{pmatrix} \frac{1}{(4\pi d/\lambda)} \tag{4}$$

since there is no depolarization due to free-space propagation, and the attenuation is given by Friis' law. The phase shift between between the reference points is given as $\phi = 2\pi d/\lambda$.

[4] Also, the Doppler spectrum is not necessarily reproduced correctly, as it is related to the angles at the MS - a simultaneous description of ADPS at the BS and the Doppler spectrum is really a MIMO description of the channel.

B. Single scattering around BS and MS

The single-scattering processes (BS→MS-scatterers→MS, and BS→BS-scatterers→MS, see Figs. 1b and 1c) can be included by modeling the location of the scatterers around the BS and MS respectively, similar to the GSCM model. The scatterer locations determine both the DOA and the delay of the MPCs that propagate via these "local" scatterers. We are thus prescribing a probability density function $pdf_{\overrightarrow{r}_{MSscatt}}(\overrightarrow{r}_{MSscatt})$ for scatterers near the MS and similarily for those near the BS. Scatterers are placed according to these pdfs; the parameters $\tau, \Omega_{R,}, \Omega_T$ for the waves corresponding to each of the scatterers are computed from simple geometrical relationships (omitted here for space reasons).

Note that the distance of the scatterers (which determine the delays) must correspond to the physical MPCs that undergo *single* scattering. It *must not* be increased in order to accommodate delay dispersion that appears somewhere else in the propagation path (i.e., in the mechanisms described in the next subsections); as detailed at the beginning of Sec. III, placing of such equivalent scatterers is not admissible in MIMO systems. It also becomes obvious that the assumption of plane waves is not essential for the validity of our model. Scatterers can be located in the near field of the transmit or receive array; the distance determines the curvature of spherical waves originating at a scatterer.

If the scattering is specular, the amplitude matrix $\underline{a}$ for scatterers around the MS can be computed as [14]

$$\underline{a} = \begin{pmatrix} \sqrt{\rho_{VV}} & \sqrt{\rho_{VH}} \\ \sqrt{\rho_{HV}} & \sqrt{\rho_{HH}} \end{pmatrix} \frac{1}{(4\pi d_{\text{ref}}/\lambda)\left[\frac{d_{MS-MSscatt}+d_{MSscatt-BS}}{d_{\text{ref}}}\right]^{n/2}}$$

where d_{ref} is an arbitrary reference distance (typically $1m$), and ρ is the reflection (scattering) coefficient that describes the attenuation between the different polarizations (note that scattering can introduce polarization "cross-talk" between vertical V and horizontal H polarization); it can depend on frequency. It follows from the image principle that the sum of $d_{MS-MSscatt}$ and $d_{MSscatt-BS}$ is the effective distance that determines the attenuation [**?**]. For a single multipath component in free space, the propagation coefficient is $n = 2$. However, it is often convenient to describe several propagation processes by a single "effective scatterer". For example, ground reflections between BS and and the MS-scatterer could be lumped together with the direct path between BS and the MS-scatterer; in that case, the propagation coefficient n follows the classical breakpoint model ($n = 2$ up to

a breakpoint distance, and $n = 4$ beyond that point) [30]. The propagation coefficient can also be determined empirically from large-scale measurements; it might then depend on frequency, and be different for the different polarization directions.

If the scattering is diffuse, then the scatterer acts as equivalent point source with a power proportional to the distance between transmitter and scatterer. This equivalent source then radiates power that again undergoes free-space attenuation. The amplitude coefficients in that case are

$$\underline{a} = \begin{pmatrix} \sqrt{\sigma_{VV}} & \sqrt{\sigma_{VH}} \\ \sqrt{\sigma_{HV}} & \sqrt{\sigma_{HH}} \end{pmatrix} \frac{1}{\frac{(4\pi d_{\text{ref}})^2}{\lambda} \left[\frac{d_{MS-MSscatt}}{d_{\text{ref}}}\right]^{n_1/2} \left[\frac{d_{MSscatt-BS}}{d_{\text{ref}}}\right]^{n_2/2}}$$

where σ is the scattering cross section for the different polarizations. Again, the propagation coefficients are $n_1 = n_2 = 2$ in free space, and may be modified in order to represent several propagation paths jointly. For notational convenience, we henceforth describe specular and diffuse scattering using the symbol $\bigoplus$ as

$$\underline{a} = \begin{pmatrix} \sqrt{\sigma_{VV}} & \sqrt{\sigma_{VH}} \\ \sqrt{\sigma_{HV}} & \sqrt{\sigma_{HH}} \end{pmatrix} \frac{1}{\left[d_{MS-MSscatt} \bigoplus d_{MSscatt-BS}\right]^{n/2}}$$

In order to simplify the model, it is often more convenient to represent the amplitude matrix as

$$\underline{a} = \begin{pmatrix} \sqrt{t_{VV}} & \sqrt{XPD_{HV}} \\ \sqrt{XPD_{HV}} & \sqrt{t_{HH}} \end{pmatrix} \sqrt{K_{MS} P_{tot}} \tag{5}$$

Here, XPD_{HV} describes the (power) crosstalk from the horizontal to the vertical polarization (and similarily for XPD_{VH}). t_{VV} describes the relative magnitude of the power transfer in the horizontal direction, normalized so that $t_{HH} + t_{VV} = 2$; this normalization makes sure that for a single-polarization antenna, the average received power is $\sqrt{K_{MS} P_{tot}}$. Note that, depending on the propagation conditions, t_{HH} can be different from t_{VV}, and XPD_{HV} can be different from XPD_{VH}. The total received power depends on the distance between transmitter and receiver, and can be modeled empirically, e.g., by the well-known Okomura-Hata model [31] and its generalizations [32]. The phase shift introduced by the scattering can be modeled as uniformly distributed and independent for the different polarization directions, though - strictly speaking - for a given scatterer material and angle of incidence, the phase shifts are deterministically given.

The quantity K_{MS} is the relative power arriving from the MS scatterers compared to the total power. Its inverse

is proportional to the Rice factor if LOS propagation and scattering around the MS are the only occuring processes. Note that this paper uses the definition of the Rice factor equal to "power in the LOS component compared to power in the diffuse components" (another common definition is nonfading power vs. power in fading components, which can be different). It is also noteworthy that in general in a MIMO system, a single Rice factor is not sufficient for the desription of the fading. Rather, we have to distinguish between the "BS Rice factor" and the "MS Rice factor". The BS Rice factor is usually small in macrocells, but can obtain appreciable values in micro- and picocells.

Next, we investigate the number of scatterers used for the simulation. We stress that the situation is fundamentally different from "conventional" fading simulator that tries to approximate Rayleigh amplitude statistics as closely as possible [6]. In that case, the larger the number of scatterers, the better the approximation of Rayleigh fading, and only runtime considerations put an upper limit on the used number of scatterers. In MIMO systems, however, the number of scatterers is an upper limit for the number of independent data streams that can be transmitted from the transmitter to the receiver; in other words, the capacity is proportional to $\min(N_{ant,BS}, N_{ant,MS,}N_{scaatt})$. The use of an infinite number of scatterers thus leads to an overoptimistic estimate of the capacity. Thus, realistic values for the number of scatterers have to be used in the model.

Similarily, the distribution of the scatterer locations and of the scattering cross sections is more critical than in "conventional" GSCM. There, it is mostly a matter of implementation efficiency whether to prescribe a nonuniform pdf of the scatterers, combined with a constant scatterer cross section, or a uniform (within a finite region) scatterer distribution with a position-dependent scatterer cross section. In MIMO systems, we cannot freely choose between these two alternatives, but rather have to select the combination of cross section distribution and location distribution that corresponds to the physical reality - again, this determines the number of independent data streams that can be transmitted in the system.This is an issue that has hardly been addressed yet in experimental investigations; the parameter suggested in Sec.V (constant scatterer cross section) is thus rather crude.

C. Double scattering

Double scattering has a special importance in the context of MIMO systems. If the distance between the BS and the MS is much larger than the effective radius of the scatterers around the BS and MS, it can lead to the so-called "keyhole-" or "pinhole-" effect. This effect describes a situation where the channel capacity is less than one would

anticipate from the correlation matrix of the received signals (for a more detailed discussion, see [20]).

Keyholes also lead to different amplitude statistics. Each scatterer at the BS "sees" the MS scatterers effectively as (the same) point source, which has a Rayleigh amplitude statistics. This statistics multiplies the "normal" Rayleigh distribution that occurs because the signal at the MS is the overlap of the signals from the many MS-scatterers.These amplitude statistics, as well as the rank reduction, are reproduced automatically by our geometrical approach.

For the simulation of the double scattering, the scatterer locations that were obtained for the scattering around BS and MS remain valid. The angles and delays are again obtained from geometrical considerations. It is important to note that every $\Omega_{R,}$ can be associated with several Ω_T.Existing models [20] assume that waves can propagate from each BS-scatterer to each MS-scatterer with equal probability; this implies that the angular power spectra at the transmitter and receiver are separable. This assumption can be violated, e.g., when the scatterer has a smooth, well-reflecting surface (pure glass front). In that case, each scatterer near the BS will illuminate only a few scatterers near the MS - essentially with a certain angular spread that depends on the surface roughness and the dimensions of the scatterers. It seems thus advantageous to define for each BS scatterer an "illumination function" f_{illum} function, including an angular spread, that determines (together with the BS - MS distance) how many BS scatterers are illuminated by each MS scatterer (and vice versa). For specular reflectors, the illumination function can be obtained from geometrical considerations, see Fig. 2. For simplicity, a possible dependence of the illumination function on the distance MS - MS-scatterer is neglected.

The computation of the amplitude matrix can then be done according to

$$\underline{a} = \begin{pmatrix} \sqrt{\sigma_{VV,BSscatt}} & \sqrt{\sigma_{VH,BSscatt}} \\ \sqrt{\sigma_{HV,BSscatt}} & \sqrt{\sigma_{HH,BSscatt}} \end{pmatrix} \begin{pmatrix} \sqrt{\sigma_{VV,MSscatt}} & \sqrt{\sigma_{VH,MSscatt}} \\ \sqrt{\sigma_{HV,MSscatt}} & \sqrt{\sigma_{HH,MSscatt}} \end{pmatrix} \cdot \cdot \frac{f_{illum}(\overrightarrow{r}_{BSscatt}, \overrightarrow{r}_{MSscatt})}{\left[d_{MS-MSscatt} \bigoplus d_{MSscatt-BSscatt} \bigoplus d_{BSscatt-BS}\right]^{n/2}}$$

or

$$\underline{a} = \begin{pmatrix} \sqrt{t_{VV,DS}} & \sqrt{XPD_{HV,DS}} \\ \sqrt{XPD_{HV,DS}} & \sqrt{t_{HH,DS}} \end{pmatrix} f_{illum}(\overrightarrow{r}_{BSscatt}, \overrightarrow{r}_{MSscatt}) \sqrt{K_{DS}} \quad (6)$$

D. Scattering via far clusters

The next step is the inclusion of far clusters (see Fig. 3). This is especially relevant in outdoor environments. It usually requires an unobstructed view from the BS to the far scatterers, and from there to the MS. However, some scattering around the MS might still occur. Since it is single- or double scattering, we can treat the problem similar to the previous subsection. In other words, we first establish the location of the far scatterers in space, and assume that all of those are illuminated by the BS. Then, each far scatterer can illuminate the MS directly, or it can illuminate a certain (angular) range of MS scatterers. From a physical point of view, far scatterers increase both the delay and the angular dispersion. Mathematically, scattering via far clusters is the same as scattering in the local cluster; only the location of the scatterers is centered around a different position. Scattering that involves both BS-scatterers, MS-scatterers and far scatterers can usually be neglected, since it carries too little energy.

E. Waveguiding

It has been observed in several urban macro- and microcellular measurement campaigns [33], [34] that waves can be coupled into a street canyon (waveguide) either directly from the transmitter, or after reflection by near or far scatterers.

Waveguiding has the following effects:

- it increases the delay dispersion. The different waveguide modes have different propagation speeds. In a geometric-optics interpretation (which is suitable for a heavily overmoded waveguide such as a street canyon), the more reflections a ray goes through when it is bounced between the side walls of the waveguide, the longer the path it has to cover, leading to longer delays. Also, the increased number of reflections will lead to an additional attenuation, so that late-arriving components are attenuated relative to the first components. If the attenuation per reflection is constant, this results approximately in an exponentially decaying power delay profile (PDP). This is also supported by numerous measurement campaigns that have shown exponential PDP in street canyon environments.
- the transfer function matrix H_{wg} for the waveguide is rank-deficient. As mentioned above, higher-order modes are attenuated more strongly than the lower order modes. For very long waveguides, only a single mode will

thus exist at the output. This gives rise to the so-called "keyhole" effect [21]. Note that this reduction in rank occurs in a different way for propagation in the horizontal and in the vertical plane. If there is pure waveguiding along a single street or a corridor, then the rank depends on the number of modes that the street (or a corridor) can support, the relative attenuation of the modes, and the length of the street. If the waveguiding involves diffraction around one corner, then this would bring the rank (with respect to horizontal plane) to unity. Note, however, that for a typical street crossing, all four corners neighboring the intersection are involved, which tends to increase the rank.

As a first approximation, we treat delay dispersion and rank deficiency in the waveguide in a multiplicative way. Although the fact that different modes propagate with different speeds couples rank and delay dispersion, our simulations of frequency-selective MIMO channels have shown that this has negligible influence on the capacity distribution.

We model the waveguide effect by a mixed geometrical and stochastic process. The coupling into the waveguide is emulated by the placement of scatterers at the coupling points into and out of the street canyon. The scatterers are distributed uniformly over the width of a street. the propagation from the TX to those scatterers is modeled geometrically, just like in the single- and double-scattering processes described in the previous subsections.The propagation through the waveguide, however, is modeled stochastically. We start with an complex Gaussian i.i.d. matrix, and perform a singular value decomposition $H_{iid} = U\Lambda V^*$. We then introduce the concept of a rank-reducing diagonal matrix; it describes the relative attenuation of the eigenmodes due to the waveguide propagation.

$$\Lambda_{rr} = \begin{pmatrix} \exp(-\lambda/\lambda_{att}) & 0 & 0 & 0 \\ 0 & \exp(-2\lambda/\lambda_{att}) & 0 & 0 \\ 0 & 0 & \exp(-3\lambda/\lambda_{att}) & 0 \\ 0 & 0 & 0 & .... \end{pmatrix} \tag{7}$$

where the parameter λ_{att} can be different for different polarizations. Note that this is only an approximate description of the relative attenuation of the waveguide modes, as the eigenmodes of the transfer function matrix H_{iid} and the waveguide modes are normally not identical. The transfer function matrix of the propagation matrix H_{wg} that describes the propagation from each "coupling scatterer" at the waveguide input to each scatterer at the waveguide

output is thus

$$H_{wg} = U\Lambda\Lambda_{rr}V^* \tag{8}$$

The propagation from the coupling scatterers at the end of the street canyon to the receiver is again computed geometrically. We stress again that coupling into and out of the canyon (i.e., propagation from TX/RX to the coupling scatterers) can occur (i) directly, (ii) via local scatterers, or (iii) via far scatterers. The relative power of those three processes must be specified, as well as the percentage of power propagation through the waveguide compared to the total power propagating from TX to RX.

F. Diffraction

Waves can also propagate over the rooftops, being diffracted at a roofedge before reaching the mobile station. Roof edge diffraction does not lead to delay dispersion, but it does result in a rank reduction of the transfer function matrix. This happens because all multipath components go through a single point (or line) in space [21]. Note, however, that this rank reduction only applies to the vertical plane, since the roof edge is horizontal.

The roof edge diffraction can be modeled most efficiently geometrically. By specifying the location of the edge, the geometry of MPCs going through that roofedge is completely specified. Again, propagation can occur from the TX directly; via local scatterers, or via far scatterers.

G. Large-scale variations

The above description analyzed mostly the modeling of small-scale fading, using the assumption that the MPC parameters (amplitude, delay, and angle) stay constant over the range of movement of the MS. However, as the MS moves over larger distances, also the MPC parameter vary. The most important of those large-scale changes are (i) shadowing, (ii) changes in the angle spread and delay spread (iii) pathloss variations, (iv) changes in delays and angles of MPCs, (v) appearance and disappearance of clusters. Since our model has a geometric structure, the large-scale fading can be simulated by the same principles and parameter values that were used in the single-directional, cluster-based COST259 channel model [9].

H. Moving scatterers

In most channel models it is assumed that temporal variations are due solely to the movements of the MS. However, moving scatterers can also play a significant role.This is especially true for scatterers close to the mobile station. There have been investigations of the temporal Rice factor (narrow-band variations) of fixed-wireless systems [23]. These indicate that the temporal Rice factor can be as low as 5dB even for systems where both link ends are situated considerably above street level. For mobile applications, passing pedestrians and cars can have an even larger influence. Specifically, they do not only act as scatterers (contributing time-varying MPCs), but also lead to shadowing of other contributions. It is thus necessary to define the statistics of the movement (speed and relative proximity to the MS), as well as the statistics of the (electromagnetic) size of the moving scatterers. Note that joint statistics of speed and size are required, as usually pedestrians will pass by closer to other pedestrians than cars and trucks. Once those statistics are specified, the effect of movement is reproduced implicitly by our geometrical approach.

To our knowledge, a systematic measurement of the moving-scatterer statistics has not yet been done in the literature. It can be anticipated, however, that this will have a very significant effect on MIMO capacity. As the angular power spectrum is an essential parameter for the capacity, shadowing of components coming from a certain direction will have a major impact.

IV. Implementation aspects

A. Implementation recipe

Once the model parameters are known, impulse responses can be generated by simply adding up the contributions from the different propagation processes. A system simulation usually requires the transfer function matrix H for a specific antenna configuration. The properties of the MPCs $h(\tau_\ell, \Omega_{R,\ell}, \Omega_{T,\ell})$ can be computed directly from the location of the scatterers as described in Sec.III; the entries of the matrix channel transfer function can be computed from (2) for different antenna configurations. In order to facilitate the implementation of the model, this subsection provides a suggestion for a rough programming structure. To simplify the description, we assume an unpolarized case.

1) Place the BS at the center of the coordinate system. Choose location of the MS according to simulation requirements (random drop, etc.), and place centers of far scatterer clusters according to model (COST 259, etc.).
2) Generate random scatterer locations according to $pdf_{BS,MS,fs}(r, \varphi, z)$. Generate (random or deterministic) scattering cross sections according to prescribed $pdf_{\sigma}(\sigma)$.
3) Place the roofedge at height and distance from MS that is typical in the considered environment.
4) Compute delay and direction of LOS component from the geometry; amplitude from (4), compute the contribution to h_{ij} from (2) (this step is required for all the points below and will not be mentioned explicitly anymore).
5) Compute the delay and directions of components created by single scattering around the MS from the geometry; determine the amplitude from (5). Do the same for single scattering near the BS, and far scatterers.
6) From the illumination function, determine (geometrically) which BS scatterer is illuminated by which MS scatterer.
7) Compute the delay and directions of the double-scattering components (for BS-scatterers - MS-scatterers, for MS-scatterers - far scatterers, and BS-scatterers - far-scatterers); compute their amplitudes from Eq. 6.
8) Rooftop edge: compute the intersection of all considered rays with a vertical wall at the edge's position. The horizontal coordinates of those intersection points are stored as $x_{edge,}y_{edge.}$ This, together with the height of the edge z_{edge}, specifies the points through which the rays have to pass. For example, the (quasi) LOS component goes from the BS to the point $x_{edge,}y_{edge,}z_{edge}$, and from there to the MS. The requirement to pass through the edge can be valid for all propagation paths, or only for some of them (e.g., it could be imposed for the LOS component and the scattering around the BS and the associated double-scattering processes, but not for far-scatterer processes).
9) Waveguide:
    a) define location of "coupling scatterers" at the entrence of the waveguide (uniform across waveguide width, which is identical to street width), both for the coupling near the BS, and the MS Compute propagation matrix $\underline{H}_{coup,BS}$ from the BS to the BS-coupling scatterers, and $\underline{H}_{coup,MS}$ from the MS

to the MS-coupling scatterers. The number of those scatterers N_{coup} should be at least as large as $N_{BSscatt}$, $N_{MSscatt}$.

b) generate a $N_{coup} \times N_{coup}$ iid complex Gaussian matrix, perform an eigendecomposition.The transfer function matrix describing the waveguide is given by 8 and 7.

c) the total contribution from a waveguide is $\underline{H}_{coup,BS} H_{wg} \underline{H}_{coup,Ms} \exp(-\tau/\nu)$.

10) Normalize each of the above contributions to unit energy, then weigh them their appropriate relative weights P, and sum them up.

11) Move the MS, and possibly the scatterers, incrementally (to simulate the temporal evolution of the channel), or re-initialize all random parameters (for a new "drop" of the MS).

B. Parameter values and capacities for macro- and microcells

In the previous sections we have discussed the basic propagation processes, and the implementation of the model derived from these. In the current section, we discuss a possible set of actual parameter values. We stress that this is done only to exemplify the basic structure of the model and to indicate a reasonable range of parameters. For better parameterizations, many extensive measurement campaigns will be needed in the future.

The full tables of the parameters and their proposed values are given in Table I. For simplicity, we assume that all parameters are independent of polarization. In macrocells, scattering around the BS is rare, which is why the power carried by scattering near the BS has been set to zero. The effective radius of the scatterers around the MS has been chosen as $100m$ for the macrocell, and $30m$ for the microcell. This corresponds well both with physcial intuition, and with observed decay time constants in those environments. We assume a Gaussian distribution of scatterers locations, and a scatterer cross section that is independent of location. However, we stress that the question of how the scatterer locations and cross sections are distributed has not been measured yet.

In macrocells, the angular spread is mainly determined by the occurrence of far clusters. Typical Urban environments (with a small number of far clusters, and a relatively small power carried by that cluster: $-10dB$ was chosen here) thus exhibit a high correlation of the signals at the BS, leading to lower capacities. The Rice factor was chosen to be higher in microcells, as a true line-of-sight situation is more probable there than in macrocells.

As far as keyhole effects are concerned, over-the-rooftop propagation is of greater importance in macrocells, so that vertical antenna arrangements are affected by the keyhole effect. Waveguiding, which can give rise to keyholes for horizontal antenna arrangements, is also important: we chose one roofedge and two waveguides as typical setting [33]. The delay dispersion of a waveguide was set to $200ns$, whereas a roof edge does not introduce delay dispersion. We also assume that roof edges lead to a strong rank reduction (for vertical arrangements), whereas waveguides imply a "softer" degradation of the rank.

For the shadowing, we *assume* independent fading of each cluster, as in the COST259 model. The shadowing per cluster is characterized by the shape of the probability density function (assumed to be lognormal), the variance (typically on the order of $3-10$ dB), and the coherence length anywhere from 5 to 100 m). The pathloss is assumed to follow the model of COST231 [32] for macrocells, and [35] for microcells.

Based on the generic model structure and the parameterization presented here, we have developed a simulation program for the generation of impulse responses in the different environments. From these, we can derive the cumulative distribution functions (cdf) of the information-theoretic capacities according to[2]

$$C = \log_2 \left[\det \left(I_{N_{\mathrm{r}} * N_{\mathrm{r}}} + \frac{\overline{\Gamma}}{N_{\mathrm{t}}} \underline{H} \underline{H}^H \right) \right]$$

where $I_{N_{\mathrm{r}} * N_{\mathrm{r}}}$ is the $N_{\mathrm{r}} * N_{\mathrm{r}}$ identity matrix and $\overline{\Gamma}$ is the mean signal-to-noise ratio (SNR) per receiver branch.

Figure 5 shows an example in both a macro- and microcellular environment. We compare curves for a 4×4 system at $15dB$ SNR in a macro- and a microcellular environment. For macrocells, a distance of $2000m$ was assumed, while for the microcell, $500m$ are used. We also show the cdf for a simple channel, namely the independent Rayleigh fading at all antenna elements. We see that the loss in outage capacity (compared to the ideal case) is on the order of 40% for macrocells, and 30% for microcells if the antenna elements are spaced half a wavelength apart. The higher loss in macrocells is mainly due to the correlation between the signals at the BS. This is also confirmed by Fig. 4b, which shows the result for an antenna spacing of 20λ. We see that the capacity is actually slightly *larger* in the macrocell than in the microcell. Similar effects could also be achieved by polarization diversity or pattern diversity.

V. Summary and conclusion

This paper presented a generic model for MIMO wireless channels. It identified the most important propagation mechanisms, and established a physical model, taking into account the scattering near BS and MS, as well as scattering by far clusters, multiple scattering, diffraction, and waveguiding effects. Also, the fact that there is only a limited number of scatterers is taken into account. All these effects contribute to eigenvalue distributions that are different from those of an independent Rayleigh-fading channel, and thus imply a lower capacity. Some exemplary capacity distribution curves, based on typical parameter choices, demonstrated those capacity losses. We also gave equations for the impulse responses as a function of the parameters, both in the double-directional formulation, and the matrix channel formulation that can be used to characterize MIMO channels.

The complete characterization of the model requires a considerable number of parameters. A full establishment of all statistical distribution of these parameters is a daunting task, and will keep experimentalists busy for many years to come. Still, we think that this is the first time that a comprehensive generic MIMO channel model has been presented, and only on this basis can a measurement program be performed and evaluated. Furthermore, the formulation of the model also allows reuse of many of the insights and data gained in previous single-directional or non-directional measurement campaigns.

Acknowledgements: The author would like to thank Dr. Jack Winters and Dr. Larry Greenstein for critical reading of the manuscript and helpful suggestions.

REFERENCES

[1] J. H. Winters, "On the capacity of radio communications systems with diversity in Rayleigh fading environments," *IEEE J. Selected Areas Comm.*, vol. 5, pp. 871–878, June 1987.

[2] G. J. Foschini and M. J. Gans, "On limits of wireless communications in a fading environment when using multiple antennas," *Wireless Personal Communications*, vol. 6, pp. 311–335, Feb. 1998.

[3] G. J. Foschini, "Layered space-time architecture for wireless communication in a fading environment when using multi-element antennas," *Bell Labs Techn. J.*, pp. 41–59, Autumn 1996.

[4] V. V. Tarokh, H. Jafarkhani, and A. R. Calderbank, "Space-time block codes from orthogonal designs," *IEEE Trans. Information Theory*, vol. 45, pp. 1456–1467, 1999.

[5] J. D. Parsons, *The mobile radio propagation channel*. Halstead Press, 1992.

[6] M. Paetzold, *Mobile Fading Channels*. Wiley, 2002.

[7] C. 207, "Digital land mobile radio communications," Tech. Rep. ISBN 92-825-9946-9, Commission of the European Union, Luxembourg, 1989.

[8] International Telecommunications Union, "Guidelines for evaluation of radio transmission technologies for imt-2000," tech. rep., 1997.

[9] M. Steinbauer and A. F. Molisch, *Directional Channel Modelling*, ch. 3.2, pp. 148–194. Wiley, 2001.

[10] D. Shiu, G. Foschini, M. .Gans, and J. Kahn, "Fading correlation and its effect on the capacity of multi-element antenna systems," *IEEE Trans. Comm.*, vol. 48, pp. 502–513, 2000.

[11] C. N. Chuah, D. N. C. Tse, J. M. Kahn, and R. A. Valenzuela, "Capacity scaling in mimo wireless systems under correlated fading," *IEEE Trans. Information Theory*, vol. 48, pp. 637 –650, 2002.

[12] W. C. Jakes, *Microwave Mobile Communications*. IEEE Press, 1974.

[13] W. C. Y. Lee, "Effects on correlation between two mobile radio base-station antennas," *IEEE Trans. Comm.*, vol. 21, pp. 1214–1224, 1973.

[14] J. Fuhl, A. Molisch, and E. Bonek, "Unified channel model for mobile radio systems with smart antennas," *IEE Proc. Radar, Sonar and Navigation*, vol. vol. 145, no. 1, pp. 32–41, 1998.

[15] H. Boelcskei, D. Gesbert, and A. J. Paulraj, "On the capacity of OFDM-based multi-antenna systems," in *Proc. IEEE ICASSP 2000*, p. to appear, 2000.

[16] TSG RAN WG4, "Deployment aspects," Tech. Rep. 3G TR 25.493 V2.0.0, 3rd Generation Partnership Project (3GPP), 2000.

[17] J. P. Kermoal, L. Schumacher, K. Pedersen, P. E. Mogensen, and F. Frederiksen, "A stochastic mimo radio channel model with experimental validation," *IEEE J. Selected Areas Comm.*, vol. 20, pp. 1211–1226, 2002.

[18] K. Y. andB. Ottersten, "Models for mimo propagation channels - a review," *J. of Wireless Communications and Mobile Computing*, Oct. 2002.

[19] A. Abdi and M. Kaveh, "A space-time correlation model for multielement antenna systems in mobile fading channels," *IEEE J. Selected Areas Comm.*, vol. 20, pp. 550–560, 2002.

[20] D. Gesbert, H. Bolcskei, D. Gore, and A. J. Paulraj, "MIMO wireless channels: Capacity and performance prediction," in *Proc. Globecomm 2000*, (San Francisco), pp. 1083–1088, IEEE, 2000.

[21] D. Chizhik, G. J. Foschini, and R. A. Valenzuela, "Capacities of multi-element transmit and receive antennas: Correlations and keyholes," *Electronics Lett.*, vol. 36, pp. 1099 –1100, 2000.

[22] T. Svantesson, "A physical mimo radio channel model for multi-element multi-polarized antenna systems," in *Proc. VTC fall 2001*, pp. 1083–1087, 2001.

[23] P. Soma, D. S. Baum, V. Erceg, R. Krishnamoorthy, and A. J. Paulraj, "Analysis and modeling of multiple-input multiple-output (mimo) radio channel based on outdoor measurements conducted at 2.5 ghz for fixed bwa applications," in *Proc. ICC2002*, pp. 272–276, 2002.

[24] M. Steinbauer, A. F. Molisch, and E. Bonek, "The double-directional radio channel," *IEEE Antennas and Propagation Mag.*, pp. 51–63, August 2001.

[25] A. M. Sayeed, "Deconstructing multiantenna fading channels," *IEEE Trans. Signal Processing*, vol. 50, pp. 2563 –2579, 2002.

[26] J. C. Liberti and T. S. Rappaport, "A geometrically based model for line-of-sight multipath radio channels," pp. 844–848, 1996.

[27] P. Petrus, J. H. Reed, and T. S. Rappaport, "Geometrical-based statistical macrocell channel model for mobile environments," *IEEE Trans. Communications*, vol. 50, pp. 495 –502, 2002.

[28] J. Blanz, P. Baier, and P. Jung, "A flexibly configurable statistical channel model for mobile radio systems with directional diversity," in *Proc. 2. ITG Fachtagung Mobile Kommunikation*, (Neu-Ulm), pp. 93–100, ITG, Sept 1995.

[29] A. Molisch, J. Laurila, and A. Kuchar, "Geometry-base stochastic model for mobile radio channels with directional component," *Proc. 2nd Intelligent Antenna Symp., Univ. Surrey*, 1998.

[30] T. S. Rappaport, *Wireless Communications Principles and Practice*. IEEE Press, 1996.

[31] M. Hata, "Empirical formulas for propagation loss in land mobile radio service," *IEEE Transactions on Vehicular Technology*, pp. 317–325, 1980.

[32] E. Damosso and L. C. (Ed.), "Digital mobile radio: COST 231 view on the evolution towards 3rd generation systems," *COST 231 Final Report*, 1999.

[33] M. Toeltsch, J. Laurila, A. F. Molisch, K. Kalliola, P. Vainikkainen, and E. Bonek, "Spatial characterization of urban mobile radio channels," in *Proc. VTC 2001 Spring*, pp. 204–208, 2001.

[34] A. Kuchar, J. P. Rossi, and E. Bonek, "Directional macro-cell channel characterization from urban measurements," *IEEE Trans. Antennas Prop.*, vol. 48, pp. 137 –146, 2000.

[35] M. J. Feuerstein, K. L. Blackard, T. S. Rappaport, S. Y. Seidel, and H. H. Xia, "Path loss, delay spread, and outage models as functions of antenna height for microcellular system design," *IEEE Transactions on Vehicular Technology*, vol. VT-43, no. 3, pp. 487–498, 1994.

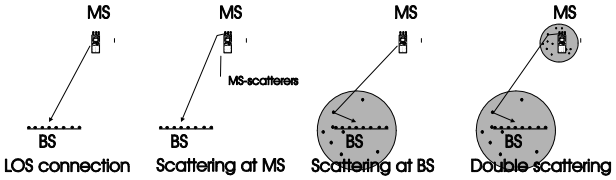

Fig. 1. Scattering around BS and MS.

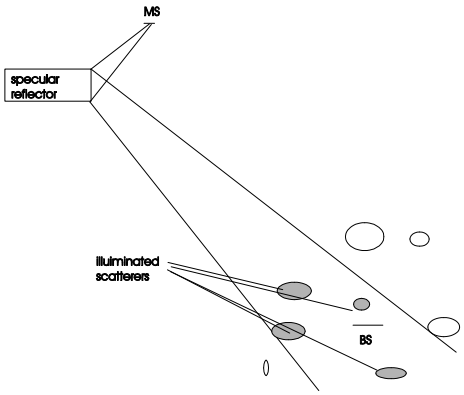

Fig. 2. Computation of illumination function for specular reflector.

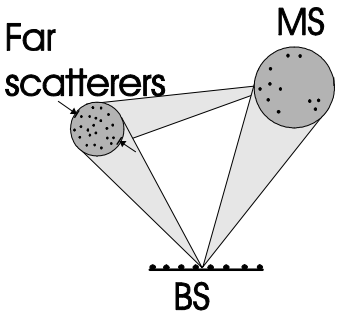

Fig. 3. Scattering via far clusters

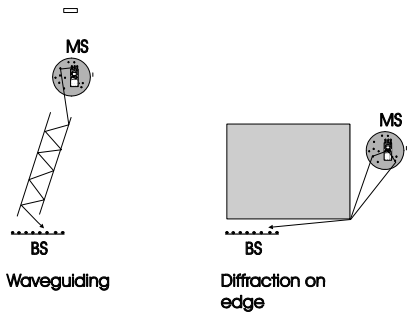

Fig. 4. Waveguiding and diffraction.

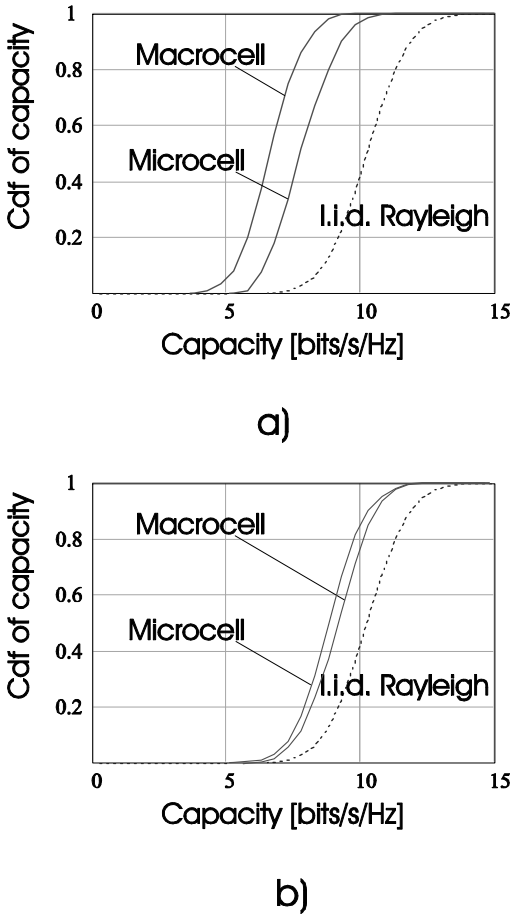

Fig. 5. Cumulative distribution function of capacity of a 4×4 MIMO system in different channels: macrocellular, microcellular, and independent Rayleigh fading at all antenna elements. System parameters: $10dB$ SNR; antenna distance 0.5λ (a) or 20λ (b) at BS and MS.

variable	Macrocell	Microcell	meaning
$P_{NB\text{-}NLOS}$	COST231-Hata	Feuerstein	Narrowband power carried by non-LOS contributions
K_{Rice}	-10dB	-3dB	Rice factor
$N_{BSscatt}$	4	8	Number of scatterers around BS
$pdf_{BS}(r,\varphi, z)$	$\frac{1}{10}\exp(-r^2/2\cdot 100^2)$ *for* $-5 < z < 5$	$\frac{1}{10}\exp(-r^2/2\cdot 30^2)$ *for* $-5 < z < 5$	Distribution of scatterers around BS
$P_{BSscatt}$	$-\infty dB$	-10dB	Power carried by BS scatterers if all are illuminated uniformly by a source at the MS (relative to $P_{NB\text{-}NLOS}$)
$N_{MSscatt}$	12	12	Number of scatterers around MS
$pdf_{MS}(r,\varphi, z)$	$\frac{1}{15}\exp(-r^2/2\cdot 100^2)$ *for* $-5 < z < 10$	$\frac{1}{15}\exp(-r^2/2\cdot 30^2)$ *for* $-5 < z < 10$	Distribution of scatterers around MS
$P_{MSscatt}$	-2.2dB	-6dB	Power carried by MS scatterers if all are illuminated uniformly by a source at the BS (relative to $P_{NB\text{-}NLOS}$)
$P_{doublescatt}$	$-\infty dB$	-13dB	power carried by MPCs that are scattered by scatterers both near the MS and BS
$\varphi_{mean,illum}$	Uniform in seen region	Uniform in seen region	Mean of the illumination angle of scatterers at MS by scatterers at BS and vice versa
$\varphi_{spread,illum}$	2 degrees	5 degrees	Spread of the illumination angle of scatterers at MS by scatterers at BS and vice versa
N_{fc}	1	1	Number of far clusters
N_w	*3* (one roofedge, 2 waveguides)	*5* (waveguides)	Number of waveguides and edges
For each far cluster			
$N_{fcscatt}$	10	10	Number of scatterers in the far cluster
$pdf_{fc}(r,\varphi,z)$	$\exp(-(r-r_0)^2/2\cdot 100^2)$ location of cluster centers uniform in cell	$\exp(-(r-r_0)^2/2\cdot 100^2)$ location of cluster centers uniform in cell	Distribution of scatterers in the far cluster
P_{fc}	-10dB	-10dB	power carried by the far cluster (relative to $P_{NB\text{-}NLOS}$)
$P_{fc\text{-}BSscatt}$	$-\infty dB$	-10dB	Power carried by MPCs that go via BS-scatterer (relative to P_{fc})
$P_{fc\text{-}MSscatt}$	-7dB	-7dB	power carried by MPCs that go via MS-scatterer (relative to P_{fc})
$\varphi_{spread,illum,fcBS}$	All scatterers illuminated	All scatterers illuminated	Spread of the illumination angle of scatterers at BS by far scatterers and vice versa
$\varphi_{spread,illum,fcMS}$	All scatterers illuminated	All scatterers illuminated	Spread of the illumination angle of scatterers at MS by far scatterers and vice versa
For each waveguide			
P_w	-10dB	-10dB	
$h(\tau)$	$\exp(-\tau/\upsilon)$ ν=200ns (waveguide), 0ns (edge)	$\exp(-\tau/\upsilon)$ ν=200ns	additional time dispersion created in the waveguide
$pdf(\lambda_{i,v})$	$\exp(-\lambda/4)$	$\exp(-\lambda/2)$	Eigenvalue distribution of the propagation matrix for horizontal components
w_{street}	10m	10m	Width of the street over which "coupling scatterers" are distributed
$P_{w,BSdirect}$	-0.45dB	-3.3dB	Power coupled into the waveguide directly (relative to P_w)
$P_{w,BSscatt}$	$-\infty dB$	-3.3dB	Power coupled into waveguide via BS scatterers (relative to P_w)
$\varphi_{spread,illum,wBS}$	All scatterers illuminated	All scatterers illuminated	Angular spread of the BS scatterers that couple power into the waveguide
$P_{w,MSdirect}$	-3.3dB	-1.9dB	Power is coupled out of the waveguide directly (relative to P_w)
$P_{w,MSscatt}$	-3.3dB	-6dB	Power coupled into the waveguide via MS scatterers (relative to P_w)
$\varphi_{spread,illum,wBS}$	All scatterers illuminated	All scatterers illuminated	Angular spread of the MS scatterers that couple power into the waveguide
$P_{w,fc\text{-}BS}$	-10dB	-10dB	Power coupled into to the waveguide by each of the far scatterer clusters
$P_{w,fc\text{-}MS}$	-10dB	-10dB	

Fig. 6.